Analyst

PAPER

Ionization characteristics of amino acids in direct analysis in real time mass spectrometry†

Cite this: *Analyst*, 2014, **139**, 2589

Kanako Sekimoto,‡*[a] Motoshi Sakakura,[b] Takatomo Kawamukai,[b] Hiroshi Hike,[b] Teruhisa Shiota,[b] Fumihiko Usui,[b] Yasuhiko Bando[b] and Mitsuo Takayama[a]

Received 26th November 2013
Accepted 24th February 2014

DOI: 10.1039/c3an02193a

www.rsc.org/analyst

The positive and negative ionization characteristics of 20 different α-amino acids were investigated using Direct Analysis in Real Time (DART) mass spectrometry. Almost all of the amino acids M were ionized to generate the (de)protonated analytes $[M \pm H]^{\pm}$ *via* proton transfer reactions with the typical background ions $H_3O^+(H_2O)_n$ and $O_2^{\bullet -}$ and resonant electron capture by M. The application of DART to amino acids also resulted in molecular ion formation, fragmentation, oxidations involving oxygen attachment and hydrogen loss, and formation of adducts $[M + R]^-$ with negative background ions R^- ($O_2^{\bullet -}$, HCO_2^-, NO_2^- and $COO^-(COOH)$), depending on the physicochemical and/or structural properties of individual amino acids. The relationship between each amino acid and the ionization reactions observed suggested that fragmentation can be attributed to pyrolysis during analyte desorption as well as excess energy obtained *via* (de)protonation. Oxidation and $[M + R]^-$ adduct formation, in contrast, most likely originate from reactions with active oxygen such as hydroxyl radicals $HO^{\bullet}$, indicating that the typical background neutral species involved in analyte ionization in DART mass spectrometry contain $HO^{\bullet}$.

Introduction

The recent development of ambient desorption/ionization (ADI) mass spectrometry offers numerous advantages, including direct analysis of solids and liquids under ambient conditions with little or no sample preparation. For these reasons, ADI sources have become important tools in cleaning validation,[1] forensic analysis,[2] and drug discovery.[3] Although several different types of ADI sources have been developed so far, a large amount of interest has been placed on direct analysis in real time (DART) using a helium plasma source, which is the origin of ADI sources.[4] DART combines separate desorption and ionization processes into a single method. The desorption is carried out using hot helium gases, whereas the ionization goes through an atmospheric pressure chemical ionization (APCI)-like process with reactions involving excited helium.[5,6] It has been reported that DART is a soft ionization technique forming abundant (de)protonated analytes $[M \pm H]^{\pm}$ *via* proton transfer from background ions such as $H_3O^+(H_2O)_n$ and $O_2^{\bullet -}$ to the analytes M,[4,5] while analytes with certain specific features can be ionized to form additional analyte ions. For instance, DART ionization of nonpolar compounds such as alkanes leads to the production of analyte ions originating from hydride abstraction, oxygen attachment, or hydrogen loss, instead of $[M \pm H]^{\pm}$.[6,7] The mechanism of formation of those analyte ions is not well understood, although the involvement of NO^+, one of the background ions in DART gas flow, has been suggested.[6] A lack of knowledge concerning the ionization characteristics in DART results in difficulty in the interpretation of DART mass spectra and limits its analytical utility. In order to overcome these issues, it is necessary to investigate the ionization characteristics of DART in detail, *i.e.*, to identify the background ionic and neutral species formed in DART sources and to systematically understand the influence of these individual background compounds on analyte ionization.

Herein, the positive and negative ionization characteristics of 20 different α-amino acids were investigated by DART mass spectrometry. The amino acids used have a wide variety of physicochemical and/or structural properties originating from their side chains, including the nonpolarity associated with the aliphatic or aromatic character and the polarity due to the presence of specific functional groups (hydroxyl, amino, carboxyl and thiol groups). All of the amino acids except arginine were positively and negatively ionized *via* various different reactions including (de)protonation, molecular ion formation, fragmentation, oxidation, hydrogen loss, and the formation of adducts with negative background ions. The relationship between the physicochemical and/or structural properties of the individual amino acids and ionization reactions observed contributes to the understanding of the formation of background ionic and neutral species and the resulting effects on analyte ionization in DART.

[a]*Graduate School of Nanobioscience, Yokohama City University, 22-2 Seto, Kanazawa-ku, Yokohama, Kanagawa, 236-0027 Japan. E-mail: sekimoto@yokohama-cu.ac.jp; Tel: +81-45-787-2216*

[b]*AMR Inc., 13-18 Nakane-2, Meguro-ku, Tokyo, 152-0031 Japan*

† Electronic supplementary information (ESI) available. See DOI: 10.1039/c3an02193a

‡ Present address: Graduate School of Nanobioscience, Yokohama City University, 22-2 Seto Kanazawa-ku, Yokohama, Kanagawa, 236-0027 Japan.

Experimental

All mass spectra were acquired with an LCQ ion-trap mass spectrometer (Thermo Fisher Scientific, San Jose, CA) equipped with a DART-SVP source (IonSense, Saugus, MA). The DART-SVP source was operated with a needle voltage of 5000 V and an exit grid electrode voltage of 350 V. Helium (He) at 350 °C was used for the DART gas at the factory-preset flow rate (2.5 L min^{-1}). The DART source exit was directed toward the orifice of the mass spectrometer, separated by a gap of ≈10 mm. The analytes used were 20 standard α-amino acids (Table 1), purchased from Sigma-Aldrich (Tokyo, Japan). Analyte desorption and ionization were accomplished by the insertion of a 1.5 mm i.d. glass tube containing the analyte in the He gas flow between the DART source exit and the mass spectrometer orifice. The resulting gas-phase analyte ions were introduced into the orifice. The orifice was heated at 275 °C and applied a voltage of 20 V. The ions were focused onto the skimmer and the tube lens and were transported into the ion-trap analyzer through ion guides consisting of a quadrupole, gate lens, octapole and entrance lens. The voltages applied to the skimmer and tube lens were 0 and 50 V, respectively. The applied RF voltages on the quadrupole and octapole were 400 V peak-to-peak. The gate lens regulating the ion injection into the ion-trap analyzer utilized an applied voltage of 16 V, whereas the voltage on the entrance lens for the eventual focusing of the transported ions was 30 V.

Results and discussion

(De)protonation

The positive- and negative-ion DART mass spectra of Asn (Mr 132) shown in Fig. 1 are representative examples. The mass spectra show the dominant ion peaks of the (de)protonated analytes $[Asn \pm H]^{\pm}$, which are the major ion species commonly observed when ionizing various other amino acids. The ion species observed in the DART mass spectra of each of the amino acids are summarized in Table 1. The protonated analytes $[M + H]^+$ are most likely produced *via* proton transfer reactions involving $H_3O^+(H_2O)_n$, the typical positive background ions in DART.[4] Proton affinities of analytes M used[8] are higher than that of H_2O (691.0 kJ mol^{-1})[8] and its clusters $(H_2O)_n$, as listed in Table 1.

$$M + H_3O^+(H_2O)_n \rightarrow [M + H]^+ + (H_2O)_{n+1} \quad (1)$$

The reactant ions $H_3O^+(H_2O)_n$ can be formed *via* Penning ionization to form $H_2O^{\bullet+}$ (reaction (2)), due to the energy transfer from an excited He atom with 19.8 eV excitation energy, $He(2^3S)$, to H_2O having an ionization energy of 12.6 eV, and subsequent reactions involving additional H_2O (reactions (3) and (4)).

$$He(2^3S) + H_2O \rightarrow H_2O^{\bullet+} + He(1^1S) + e_{slow}^- \quad (2)$$

$$H_2O^{\bullet+} + H_2O \rightarrow H_3O^+ + HO^{\bullet} \quad (3)$$

$$H_3O^+ + (H_2O)_n \rightarrow H_3O^+(H_2O)_n \quad (4)$$

In contrast, the formation of deprotonated analytes $[M - H]^-$ are most likely attributed to two different processes, *i.e.*, proton transfer from analytes M to the negative background ions $O_2^{\bullet-}$ (ref. 5) and resonant electron capture by M. The $O_2^{\bullet-}$ ions are formed *via* attachment of thermal electrons having kinetic energies at ambient temperature, *i.e.*, e_{slow}^- (≈0 eV) to O_2 (reaction (5)):

$$O_2 + e_{slow}^- (\approx 0\ eV) + P \rightarrow O_2^{\bullet-} + P\ (P: N_2, O_2) \quad (5)$$

where P represents common air constituents such as N_2 and O_2 corresponding to a third body. Slow electrons e_{slow}^- with low kinetic energies can be produced *via* Penning ionization (reactions (2), (10) and (12)) and/or the following surface Penning ionization (reaction (6)).[5]

$$He(2^3S) + surface \rightarrow He(1^1S) + surface + e_{fast}^- \quad (6)$$

The electrons formed *via* reaction (6), e_{fast}^-, are rapidly thermalized by collisions with common air constituents P (reaction (7)).

$$e_{fast}^- + P \rightarrow e_{slow}^- + P\ (P: N_2, O_2) \quad (7)$$

The collision of $O_2^{\bullet-}$ with analytes M efficiently bring about the formation of $[M - H]^-$ *via* proton transfer from M to $O_2^{\bullet-}$ (reaction (8)), due to higher proton affinity of $O_2^{\bullet-}$ (1477 ± 2.9 kJ mol^{-1})[15] rather than $[M - H]^-$.[9,10]

$$M + O_2^{\bullet-} \rightarrow [M - H]^- + HO_2^{\bullet} \quad (8)$$

The slow electrons having kinetic energies over the range of 1–1.5 eV, e_{slow}^- (1–1.5 eV), can also resonantly attach to analytes M and subsequent dehydrogenation leads to produce $[M - H]^-$ (reaction (9)).

$$M + e_{slow}^-(1\text{–}1.5\ eV) \rightarrow M^{\bullet-}* \rightarrow [M - H]^- + H^{\bullet} \quad (9)$$

The formation of deprotonated amino acids $[M - H]^-$ *via* reaction (9) has been previously reported by numerous studies regarding resonant electron capture and dissociative electron attachment using low energetic electrons.[16–20] On the basis of those previous studies, the $[M - H]^-$ ions resulting from reaction (9) have carboxylate anion structures occurring *via* either electron capture into the π* orbital of the carboxylic group[18] or hydrogen-atom tunneling through the barrier that separates a dipole-supported minimum and repulsive valence state.[19]

In order to confirm whether both proton transfer with $O_2^{\bullet-}$ (reaction (8)) and resonant electron capture (reaction (9)) are involved in deprotonation of various analytes in DART, some analytes were ionized in the analyte ionization area under N_2 atmosphere conditions. It can be expected that N_2 atmosphere conditions where few amounts of O_2 are present result in the inhibition of the occurrence of reaction (8) involving $O_2^{\bullet-}$. The mass spectra of Gly, Val, Asp and Phe, arbitrary selected, obtained under N_2 atmosphere conditions, certainly showed the ion peaks of deprotonated analytes $[M - H]^-$ for individual

Table 1 Ion species and their relative abundances observed in the DART mass spectra of individual amino acids (Fig. 1–3 and S1–S16†)

					Positive ions (relative abundances [%])				Negative ions (relative abundances [%])									
					Ionization reactions				Ionization reactions									
	Analyte (M)	Proton affinities of M and $[M-H]^-$ [kJ mol^{-1}]	Ionization energy [eV]	Dipole moment[14] [Debye]	Proto-nation	Molecular cation formation	Fragmen-tation	Oxidation	Deprotonation	Molecular –anion formation	Fragmen-tation	Oxidation	Hydrogen loss	Attachment of negative background ions R^-				
														R^-	O_2^-	HCO_2^-	NO_2^-	$COO^-(COOH)$
Aiphatic amino acids	1. Glycine (Gly: Mr 75) 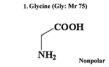	886.5[8] 1434.0 ± 9.2[9]	8.9[11]	1.33	$[M+H]^+$ (100)	$M^{\bullet+}$ (2.0)	—	—	$[M-H]^-$ (100)	—	—	—	$[M-2H-H]^-$ (20.0)	—	$[M+O_2]^-$ (2.5)	—	—	$[M+COO(COOH)]^-$ (14.6)
	2. L-Alanine (Ala: Mr 89) 	901.6[8] 1430.0 ± 7.9[9]	8.9	1.40	$[M+H]^+$ (100)	$M^{\bullet+}$ (2.4)	—	—	$[M-H]^-$ (100)	—	—	—	$[M-2H-H]^-$ (33.0)	—	$[M+O_2]^-$ (3.9)	$[M+HCO_2]^-$ (2.5)	—	$[M+COO(COOH)]^-$ (29.5)
	3. L-Valine (Val: Mr 117) 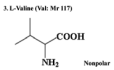	910.6[8] 1420.0 ± 13.0[10]	8.7[12]	1.40	$[M+H]^+$ (100)	$M^{\bullet+}$ (1.9)	—	—	$[M-H]^-$ (100)	—	—	—	$[M-2H-H]^-$ (22.7)	—	$[M+O_2]^-$ (11.6)	$[M+HCO_2]^-$ (5.2)	$[M+NO_2]^-$ (2.7)	$[M+COO(COOH)]^-$ (17.3)
	4. L-Leucine (Leu: Mr 131) 	914.6[8] 1418.0 ± 13.0[10]	8.5[12]	1.20	$[M+H]^+$ (100)	$M^{\bullet+}$ (2.4)	—	—	$[M-H]^-$ (100)	—	—	—	$[M-2H-H]^-$ (24.5)	—	$[M+O_2]^-$ (17.4)	$[M+HCO_2]^-$ (11.9)	$[M+NO_2]^-$ (9.1)	$[M+COO(COOH)]^-$ (43.7)
	5. L-Isoleucine (Ile: Mr 131) 	917.4[8] 1417.0 ± 13.0[10]	8.7[12]	1.36	$[M+H]^+$ (100)	$M^{\bullet+}$ (1.9)	—	—	$[M-H]^-$ (100)	—	—	—	$[M-2H-H]^-$ (26.6)	—	$[M+O_2]^-$ (19.7)	$[M+HCO_2]^-$ (9.7)	$[M+NO_2]^-$ (5.8)	$[M+COO(COOH)]^-$ (27.0)
	6. L-Serine (Ser: Mr 105) 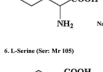	914.6[8] 1392.0 ± 13.0[10]	8.7[11]	1.96	$[M+H]^+$ (100)	$M^{\bullet+}$ (1.2)	—	—	$[M-H]^-$ (100)	—	—	—	$[M-2H-H]^-$ (5.8)	—	$[M+O_2]^-$ (1.2)	—	—	$[M+COO(COOH)]^-$ (5.3)
	7. L-Threonine (Thr: Mr 119) 	922.5[8] 1389.0 ± 13.0[10]	≤10.2[11]	2.28	$[M+H]^+$ (100)	$M^{\bullet+}$ (1.0)	—	—	$[M-H]^-$ (100)	—	—	—	$[M-2H-H]^-$ (10.6)	—	$[M+O_2]^-$ (1.5)	—	—	$[M+COO(COOH)]^-$ (6.6)
	8. L-Asparagine (Asn: Mr 132) 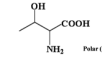	929.0[8] 1387.0 ± 13.0[10]	—	2.93	$[M+H]^+$ (100)	$M^{\bullet+}$ (1.4)	$[M+H-H_2O]^+$ (3.7)	—	$[M-H]^-$ (100)	$M^{\bullet-}$ (6.7)[a]	$[M-H-NH_3]^-$ (9.3)	—	$[M-2H-H]^-$ (4.0)	—	—	—	—	$[M+COO(COOH)]^-$ (14.9)
	9. L-Glutamine (Gln: Mr 146) 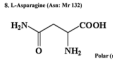	937.8[8] 1387.0 ± 13.0[10]	—	3.44	$[M+H]^+$ (100)	$M^{\bullet+}$ (2.4)	$[M+H-NH_3]^+$ ($[PGA+H]^+$) (21.8)	—	—	—	$[M-H-NH_3]^+$ ($[PGA-H]^+$) (100)	—	—	—	—	—	—	—
	10. L-Lysine (Lys: Mr 146) 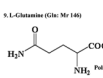	996.0[8] 1411.0 ± 13.0[10]	8.6[11]	2.43	$[M+H]^+$ (100)	$M^{\bullet+}$ (1.2)	—	—	$[M-H]^-$ (100)	$M^{\bullet-}$ (6.2)[a]	—	—	—	—	$[M+O_2]^-$ (69.3)	$[M+HCO_2]^-$ (34.2)	$[M+NO_2]^-$ (25.0)	$[M+COO(COOH)]^-$ (26.8)
	11. L-Arginine (Arg: Mr 174) 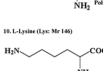	1051.0[8] 1388.0 ± 13.0[10]	—	2.25	—	—	—	—	—	—	—	—	—	—	—	—	—	—
	12. L-Aspartic acid (Asp: Mr 133) 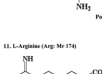	908.9[8] —	—	2.28	$[M+H]^+$ (100)	$M^{\bullet+}$ (2.4)	—	—	$[M-H]^-$ (100)	$M^{\bullet-}$ (14.6)[a]	—	—	—	—	—	—	—	—
	13. L-Glutamic acid (Glu: Mr 147) 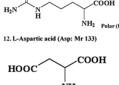	913.0[8] —	—	1.89	$[M+H]^+$ (100)	$M^{\bullet+}$ (5.4)	$[M+H-H_2O]^+$($[PGA-H]^+$) (1.1)	—	$[M-H]^-$ (100)	—	$[M-H-H_2O]^+$($[PGA-H]^+$) (8.8)	—	—	—	—	—	—	—

[a] Relative abundance of the negative ion whose *m*/*z* corresponds to the molecular mass of analyte M subtracted that of $[M-H]^-$ having one isotope of ^{13}C, ^{2}H, ^{17}O or ^{15}N.

Table 1 (*Contd.*)

					Positive ions (relative abundances [%])				Negative ions (relative abundances [%])								
					Ionization reactions				Ionization reactions					Attachment of negative background ions R^-			
	Analyte (M)	Proton affinities of M and $[M-H]^-$ [kJ mol^{-1}]	Ionization energy [eV]	Dipole moment[14] [Debye]	Proto-nation	Molecular cation formation	Fragmen-tation	Oxidation	Deprotonation	Molecular –anion formation	Fragmen-tation	Oxidation	Hydrogen loss	R^-	O_2^-	HCO_2^-	NO_2^-	$COO^-(COOH)$
Sulfur-containing aliphatic amino acids	14. L-Methionine (Met: Mr 149) 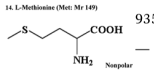 Nonpolar	935.4[8]	8.3[11]	1.84	$[M+H]^+$	$M^{\cdot+}$	—	$[M+H+O]^+$	$[M-H]^-$	—	—	$[M-H+O]^-$	$[M-2H-H]^-$	—	$[M+O_2]^-$	$[M+HCO_2]^-$	$[M+NO_2]^-$	$[M+COO(COOH)]^-$
		—			(100)	(0.7)		(5.2)	(100)			(13.4)	(30.4)		(33.2)	(11.8)	(13.9)	(113)
	15. L-Cysteine (Cys: Mr 121) 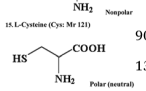 Polar (neutral)	903.2[8]	9.5[11]	1.99	$[M+H]^+$	$M^{\cdot+}$	—	—	$[M-H]^-$	—	—	—	$[M-2H-H]^-$	—	—	—	—	$[M+COO(COOH)]^-$
		1399.0 ± 9.6[10]			(100)	(1.0)			(100)				(15.6)					(19.8)
Aromatic amino acids	16. L-Phenylalanine (Phe: Mr 165) 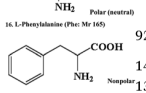 Nonpolar	922.9[8]	8.4[11]	1.32	$[M+H]^+$	$M^{\cdot+}$	—	—	$[M-H]^-$	$M^{\cdot-}$	—	$[M-H+O]^-$	$[M-2H-H]^-$	—	$[M+O_2]^-$	$[M+HCO_2]^-$	$[M+NO_2]^-$	$[M+COO(COOH)]^-$
		1408.0 ± 13.0[10]			(100)	(1.7)			(100)	(6.8)[a]		(8.7)	(14.0)		(12.0)	(7.0)	(5.3)	(15.2)
	17. L-Tyrosine (Tyr: Mr 181) 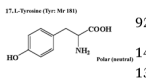 Polar (neutral)	926.0[8]	—	2.63	$[M+H]^+$	$M^{\cdot+}$	$[M+H-CO_2]^+$	$[M+H+O]^+$	$[M-H]^-$			$[M-H+O]^-$		—	$[M+O_2]^-$	$[M+HCO_2]^-$	$[M+NO_2]^-$	$[M+COO(COOH)]^-$
		1413.0 ± 13.0[10]			(100)	(1.6)	(5.9)	(4.2)	(100)	—	—	(6.3)	—	—	(63.0)	(36.1)	(30.0)	(13.2)
Heterocyclic amino acids	18. L-Proline (Pro: Mr 115) 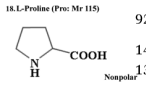 Nonpolar	920.5[8]	8.3[11]	1.64	$[M+H]^+$	$M^{\cdot+}$			$[M-H]^-$					—	$[M+O_2]^-$	$[M+HCO_2]^-$	$[M+NO_2]^-$	$[M+COO(COOH)]^-$
		1423.0 ± 13.0[10]			(100)	(0.2)	—	—	(100)	—	—	—	—	—	(24.2)	(18.2)	(6.9)	(10.1)
Aromatic heterocyclic amino acids	19. L-Tryptophane (Trp: Mr 204) 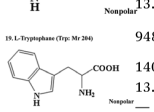 Nonpolar	948.9[8]	8.4[13]	4.18	$[M+H]^+$	$M^{\cdot+}$	—	$[M+H+O]^+$	$[M-H]^-$	—	—	$[M-H+O]^-$	—	—	$[M+O_2]^-$	$[M+HCO_2]^-$	$[M+NO_2]^-$	$[M+COO(COOH)]^-$
		1409.0 ± 13.0[10]	—	—	(100)	(2.9)	—	(8.0)	(100)	—	—	(17.1)	—	—	(62.9)	(45.6)	(37.8)	(14.7)
		—	—	—	—	—	—	$[M+H+2O]^+$	—	—	—	$[M-H+2O]^-$	—	—	—	—	—	—
		—	—	—	—	—	—	(4.1)	—	—	—	(32.7)	—	—	—	—	—	—
	20. L-Histidine (His: Mr 155) 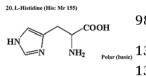 Polar (basic)	988.0[8]	—	3.91	$[M+H]^+$	$M^{\cdot+}$	—	—	$[M-H]^-$	—	—	$[M-H+O]^-$	—	—	$[M+O_2]^-$	—	—	$[M+COO(COOH)]^-$
		1385.0 ± 13.0[10]	—	—	(100)	(4.8)	—	—	(100)	—	—	(2.1)	—	—	(2.4)	—	—	(26.0)

[a] Relative abundance of the negative ion whose m/z corresponds to the molecular mass of analyte M subtracted that of $[M-H]^-$ having one isotope of ^{13}C, ^{2}H, ^{17}O or ^{15}N.

analytes M, whose absolute abundances were lower than those observed under normal ambient air conditions (Table S1 in ESI†). These results can evidence the involvement of both reactions (8) and (9) in deprotonation occurring in DART.

Molecular ion formation

Positive-ion DART brought about the formation of molecular cations $M^{\bullet+}$ for almost all the analytes M whose abundances were quite lower than those of protonated analytes $[M + H]^+$, as shown in Table 1. The $M^{\bullet+}$ formation has been reported in the previous studies of DART to analyze nonpolar compounds such as dibenzosuberone and *n*-hexadecane.[21] Taking into account the ionization energies of analytes M used, ≈9 eV (listed in Table 1),[11–13] and the previous report,[21] $M^{\bullet+}$ can be formed *via* Penning ionization involving $He(2^3S)$ (reaction (10)) and/or charge transfer reaction from $O_2^{\bullet+}$ to M (reaction (11)). The $O_2^{\bullet+}$ ion is one of the positive background ions produced *via* Penning ionization of O_2 having an ionization energy of 12.07 eV with $He(2^3S)$ (reaction (12)).[21]

$$M + He(2^3S) \rightarrow M^{\bullet+} + e_{slow}^- + He(1^1S) \quad (10)$$

$$M + O_2^{\bullet+} \rightarrow M^{\bullet+} + O_2 \quad (11)$$

$$O_2 + He(2^3S) \rightarrow O_2^{\bullet+} + e_{slow}^- + He(1^1S) \quad (12)$$

In contrast, the formation of molecular anions $M^{\bullet-}$ in negative-ion DART of a given analyte M was investigated using the abundances of the ion peak whose *m*/*z* value corresponds to the molecular mass of M and the isotopes of deprotonated analyte $[M - H]^-$. The negative-ion mass spectrum of Asn (Fig. 1b) shows the negative ion at *m*/*z* 132 with an abundance of 12.0% relative to deprotonated Asn $[Asn - H]^-$ (RA = 12.0%). The ion at *m*/*z* 132 corresponds to not only the molecular anion $Asn^{\bullet-}$ but also deprotonated Asn $[Asn - H]^-$ having one isotope of ^{13}C, ^2H, ^{17}O or ^{15}N. The calculated RA of the isotope of $[Asn - H]^-$ at *m*/*z* 132 is 5.3%. That is, the RA of $Asn^{\bullet-}$ formed in the negative-ion DART is 6.7%. The other negative-ion mass spectra obtained (Fig. 2, 3 and S1–S16†) indicated that Asp can be ionized as $Asp^{\bullet-}$ with a RA of 14.6%. In the case of Lys and Phe, the ions at *m*/*z* 146 and 165 corresponding to individual $M^{\bullet-}$ were detected at RAs of 6.2 and 6.8%, respectively (Fig. S9 and S13†). Because the mass spectra of those analytes include the ion peaks that are higher in *m*/*z* values than $M^{\bullet-}$, the ions at *m*/*z* 146 and 165 may be the fragments from the ions with higher *m*/*z* values as well as $M^{\bullet-}$. High resolution experiments with accurate mass measurement would be useful for further investigation of the molecular anion formation for Lys and Phe.

The formation of $M^{\bullet-}$ of Asn and Asp has been previously observed under low-pressure argon plasma conditions involving low energetic electrons.[16] Taking into account the

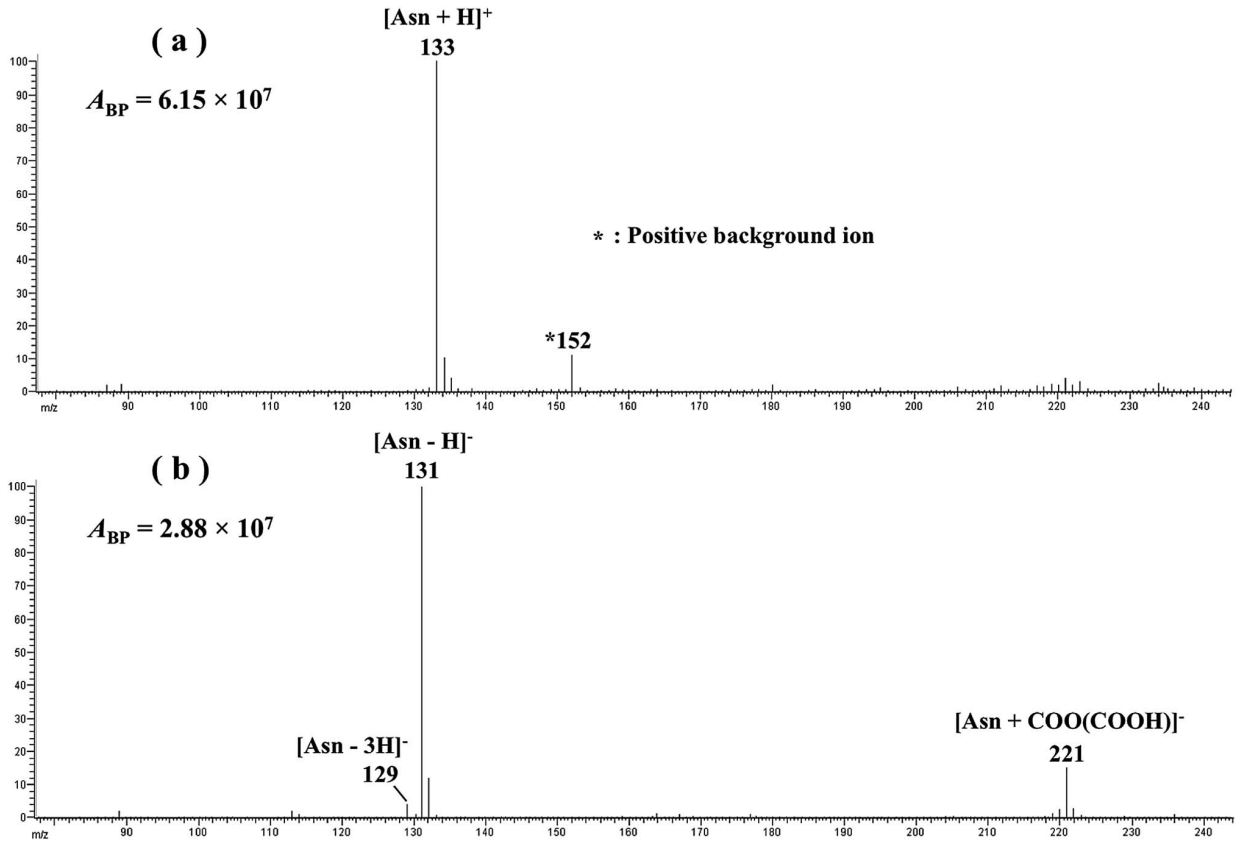

Fig. 1 (a) Positive- and (b) negative-ion DART mass spectra of L-asparagine (Asn). A_{BP} represents the absolute abundance (arbitrary units) of the base peak in each mass spectrum.

previous report, molecular anion formation occurring in DART is attributable to the resonant capture of thermal electrons e_{slow}^- ($\approx$0 eV) by analytes M and simultaneous removal of excess energy in $M^{\bullet -}$ by third bodies P such as N_2 and O_2 (reaction (13)).

$$M + e_{slow}^- (\approx 0\ eV) + P \rightarrow M^{\bullet -} + P\ (P: N_2\ and\ O_2) \quad (13)$$

It has been previously reported that analytes M having dipole moments larger than the critical magnitudes (2–2.5 Debye) are able to create the so-called dipole-bound or dipole-supported negative ion states and result in high efficiency in resonant electron capture.[19] However, the results obtained here, that Asn and Asp can more efficiently capture thermal electrons than other amino acids, cannot be explained by the dipole moments of individual amino acids in the global minimum structures.[14] For example, the dipole moment of Asp, 2.28 Debye, is equal to that of Thr, which can inefficiently capture thermal electrons. In order to understand why Asn and Asp have particularly high efficiencies in resonant electron capture, further experimental and theoretical studies will be required.

Fragmentation

Ionization of Glu and Gln, acidic and amidic amino acids, respectively, involved significant fragmentation, in which the common neutral species are lost under positive- and negative-ion modes resulting in the formation of the fragment ions with RAs higher than about 10%. Fig. 2 shows the positive- and negative-ion DART mass spectra of Glu (Mr 147). The mass spectra include the ion peaks of not only the (de)protonated Glu $[Glu \pm H]^{\pm}$ but also fragment ions corresponding to $[Glu \pm H - H_2O]^{\pm}$. It should be noted that in Fig. 2, H_2O loss fragments were observed in both positive- and negative-ion modes, indicative of the occurrence of H_2O loss, independent of ionization. It is well-known that Glu easily forms pyroglutamic acid (PGA; Mr 129) due to intramolecular thermal dehydration below 400 °C.[22] Taking into account the temperature of He gas flow used, 350 °C, the formation of $[PGA \pm H]^{\pm}$ (corresponding to $[Glu \pm H - H_2O]^{\pm}$) in DART is most likely attributable to the following processes.

(a) Initial loss of H_2O from Glu to form PGA during the thermal desorption process in the He gas stream (reaction (14)).

(b) Subsequent formation of (de)protonated PGA $[PGA \pm H]^{\pm}$ *via* proton transfer reactions of PGA with $H_3O^+(H_2O)_n$ and O_2^- (reactions (15) and (16)) and resonant electron capture by PGA (reaction (17)).

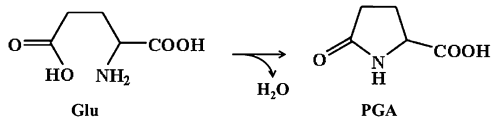

(14)

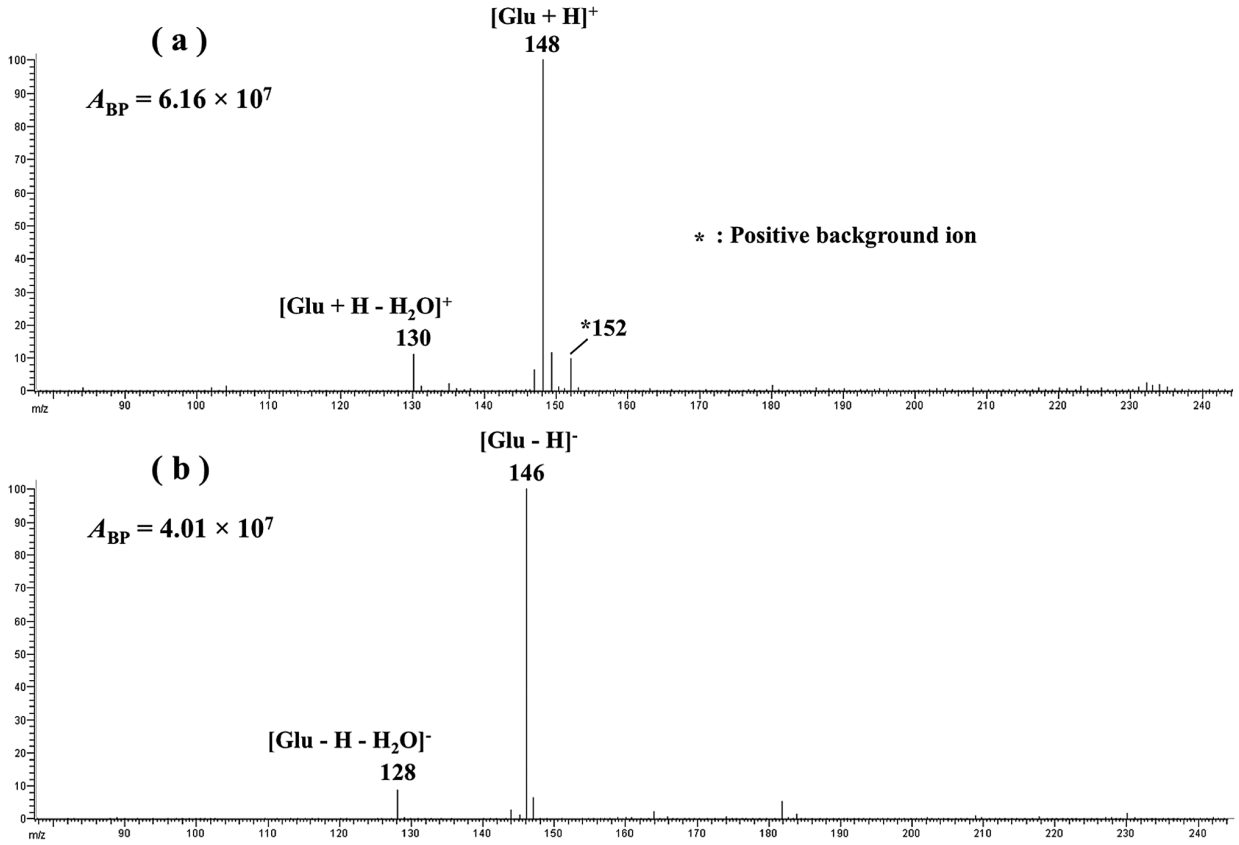

Fig. 2 (a) Positive- and (b) negative-ion DART mass spectra of L-glutamic acid (Glu). A_{BP} represents the absolute abundance (arbitrary units) of the base peak in each mass spectrum.

$$PGA + H_3O^+(H_2O)_n \rightarrow [PGA + H]^+ + (H_2O)_n \quad (15)$$

$$PGA + O_2^- \rightarrow [PGA - H]^- + HO_2 \quad (16)$$

$$PGA + e_{slow}^-(1\text{–}1.5\ eV) \rightarrow PGA^{\bullet -*} \rightarrow [PGA - H]^- + H^\bullet \quad (17)$$

Ionization of Gln led to the fragment ions of (de)protonated Gln $[Gln \pm H]^\pm$ with NH_3 loss, $[Gln \pm H - NH_3]^\pm$, which have the same *m*/*z* values as $[PGA \pm H]^\pm$ corresponding to the fragment ions of Glu (Fig. S8† and Table 1). Taking into account the pyrolysis of Gln, it can be presumed that the fragmentation processes involved in DART ionization of Gln are similar to those of Glu described above. That is, Gln can initially cyclize to pyroglutamic acid (PGA) with loss of NH_3 during thermal desorption (reaction (18)),[23] resulting in the formation of (de) protonated PGA $[PGA \pm H]^\pm$ *via* reactions (15)–(17).

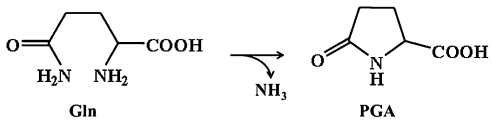

(18)

DART of the other amino acids brought about the formation of some fragment ions, *i.e.*, protonated Tyr with CO_2 loss $[Tyr + H - CO_2]^+$ (Fig. 3), protonated Asp with H_2O loss $[Asp + H - H_2O]^+$ and deprotonated Asp with NH_3 loss $[Asp - H - NH_3]^-$ (Fig. S10†), whose RAs were lower than 10%. Neutral species lost during the fragmentation in the case of Tyr and Asp are changed by varying the polarity of ionization, which suggests that those fragmentations occur due to the excess energy obtained *via* (de) protonation. The results obtained suggest, therefore, that the fragmentation occurring in DART is most likely attributable to both pyrolysis during thermal desorption and excess energy obtained *via* ionization reactions.

Oxidation

DART ionization resulted in the formation of (de)protonated analytes with the addition of one and/or two oxygens, $[M \pm H + nO]^\pm$ (n = 1, 2), for sulfur-containing, aromatic, and aromatic heterocyclic amino acids such as Met, Phe, Tyr, Trp and His (see Fig. 3 and Table 1). It has been previously reported that these five amino acids can be easily oxidized with oxygen attachment due to the hydroxyl radical HO$^\bullet$ as a strong oxidizing species, formed in ozonated solutions[24–26] or *via* Fenton reactions and/or radiolysis in aqueous solutions.[27] Scheme 1 shows oxygen addition products $[M + nO]$ of five amino acids M resulting from oxidation by HO$^\bullet$, on the basis of the previous reports.[25–27] The oxidation of Met with HO$^\bullet$ results in the formation of sulfoxide[25–27] (Scheme 1a). Reactions of HO$^\bullet$ with the aromatic rings

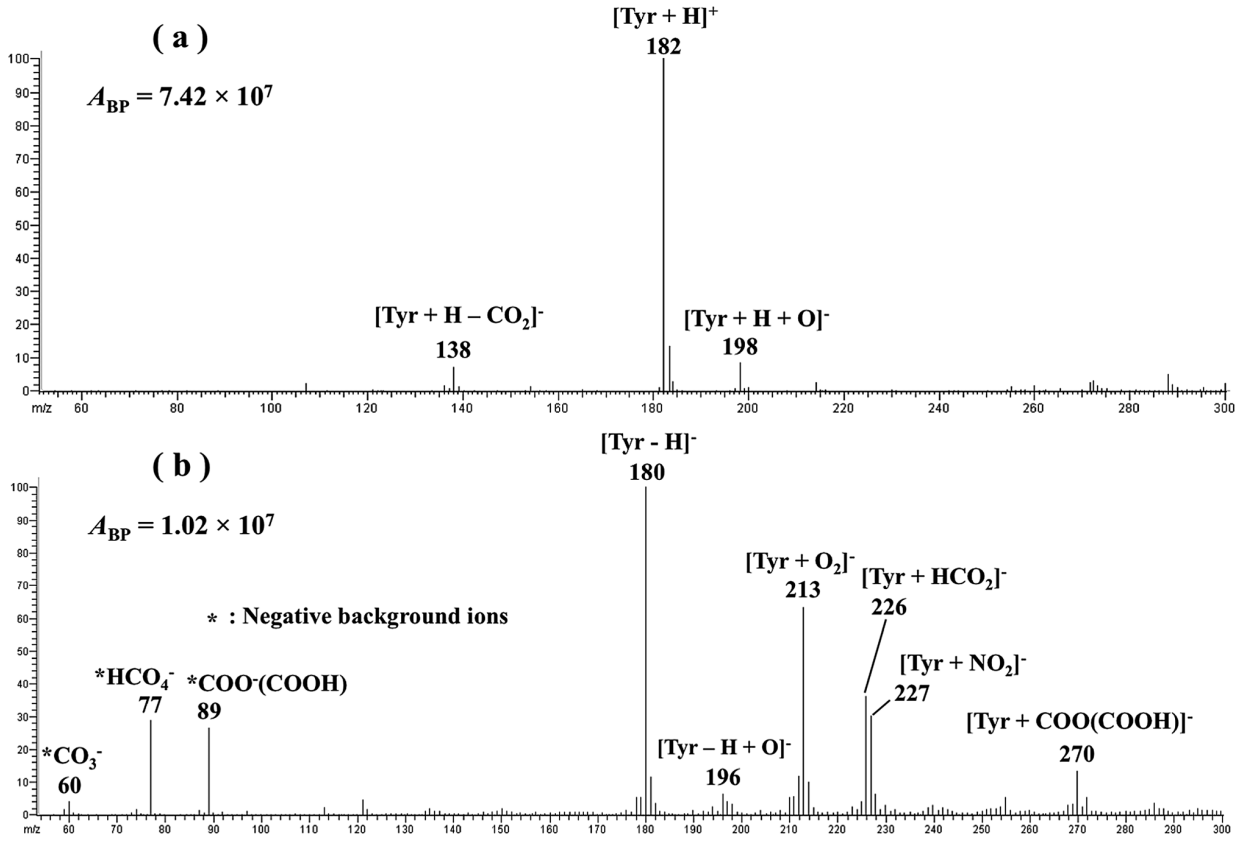

Fig. 3 (a) Positive- and (b) negative-ion DART mass spectra of L-tyrosine (Tyr). A_{BP} represents the absolute abundance (arbitrary units) of the base peak in each mass spectrum.

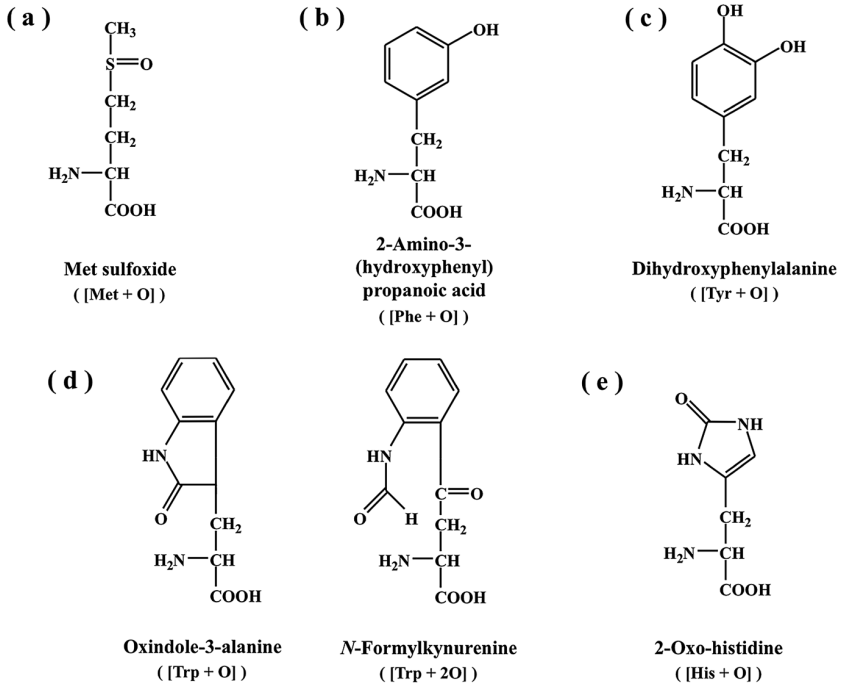

Scheme 1 Oxygen addition products of (a) methionine (Met), (b) phenylalanine (Phe), (c) tyrosine (Tyr), (d) tryptophan (Trp) and (e) histidine (His).

in Phe and Tyr lead to the addition of HO$^{\bullet}$ to the rings, and subsequent reactions of the radical species with oxygen generate 2-amino-3-(hydroxyphenyl)propanoic acid[27] and dihydroxyphenylalanine,[25,27] corresponding to the monoxides of Phe and Tyr, respectively (Schemes 1b and c). It has been reported that aromatic amino acids are oxidized to form quinones, *e.g.*, 2-amino-3-(3,4-dioxo-cyclohexa-1,5-dienyl)-propanoic acid which is a quinone structural oxidation product of Tyr.[26] However, no observation of ions related to quinones in the mass spectra of Phe and Tyr (Fig. S13† and 3) indicates less occurrence of quinone formation in DART. Trp and His can be oxidized at the conjugated double bond moiety with HO$^{\bullet}$ to form oxindole-3-alanine ([Trp + O]), *N*-formylkynurenine ([Trp + 2O]) and 2-oxo-histidine ([His + O]) (Schemes 1d and e). The oxidation reactivity of individual amino acids M can be estimated using relative abundances of $[M \pm H + nO]^{\pm}$ listed in Table 1. The reactivity order obtained here is Trp > Met > Phe > Tyr > His > other amino acids $\approx$ 0. This order is in agreement with that reported by Kotiaho *et al.* using ozonated solutions with pH 5.8: Met > Trp > Tyr > His > other amino acids.[25] In the case of higher pH conditions, oxidation of Cys to form trioxide products [Cys + 3O] proceeds most dominantly.[24,28] Taking into account the results obtained, the oxidation with oxygen attachment reactions occurring in DART most likely originate with HO$^{\bullet}$ in the ionization area under relatively acidic conditions.

Hydrogen loss

In negative-ion DART, deprotonated analytes with loss of two hydrogens, $[M - 2H - H]^{-}$, were observed when analyzing Gly, Ala, Val, Leu, Ile, Ser, Thr, Asn, Cys, Met and Phe, which have aliphatic or non-ionic side chains (see Fig. 1 and Table 1). The peak abundances from $[M - 2H - H]^{-}$ were rather low compared to the abundances of $[M - H]^{-}$. Such $[M - 2H - H]^{-}$ ions have also been observed in the negative-ion DART of aliphatic compounds such as hexanes, heptanes, cyclohexane[29] and hexatriacontane,[7] although the precise mechanism of the 2H loss reactions in DART and its dependence on the structural properties of the analytes have not yet been clarified. It has been previously reported that deprotonated Ser in aqueous solution with HO$^{\bullet}$ and O_2 loses two hydrogens from the backbone of Ser *via* sequential oxidation reactions, as shown in Scheme 2.[30] This scheme could be applied to the reactions observed here, *i.e.*, the gas-phase 2H loss from deprotonated analytes for various amino acids including Ser. In contrast, the ion peaks of $[M - 2H - H]^{-}$ have been observed in the mass spectra of Gly and Val resonantly capturing low energetic electrons ($\approx$1.5 eV).[17,20] It is likely, therefore, that the 2H loss reactions occurring in DART can be interpreted in terms of alternative oxidation processes due to HO$^{\bullet}$ and/or involvement of slow electrons e_{slow}^{-} ($\approx$1.5 eV) formed *via* reactions (2), (7), (10) and (12).

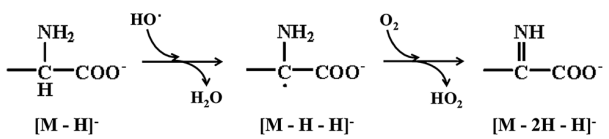

Scheme 2 Reaction of deprotonated amino acids with HO$^{\bullet}$ and O_2 to lose two hydrogens.

Formation of adducts with negative background ions

All of the amino acids M, except acidic and amidic amino acids such as Asp, Glu and Gln, formed negative ion adducts $[M + R]^-$ with background ions R^-, such as O_2^- (*m*/*z* 32), HCO_2^- (*m*/*z* 45), NO_2^- (*m*/*z* 46) and/or $COO^-(COOH)$ (*m*/*z* 89). Those ions R^- are typical negative backgrounds formed in DART. The $COO^-(COOH)$ ion can be observed in the negative-ion mass spectra of Tyr (Fig. 3b), whereas O_2^- and NO_2^- are included in a DART mass spectrum of negative background ions reported by Cody *et al.*[7] The adduct ions $[M + R]^-$ were most likely formed *via* three-body reactions with a third body P such as N_2 or O_2.

$$M + R^- + P \rightarrow [M + R]^- + P \text{ (P: } N_2, O_2) \quad (19)$$

The adduct ions $[M + R]^-$ observed are summarized in Table 1. Table 1 shows that whether $[M + R]^-$ are formed or not vary with each combination of R^- and M, which are not dependent upon the chemical properties of M, such as whether the analyte is aliphatic or aromatic or has certain functional groups. The results obtained suggest that the formation of the $[M + R]^-$ adducts is attributed to the affinity or ability of complexation between individual R^- and M, although the factors determining its affinity or ability cannot be readily proven. Similar phenomena have been also observed in atmospheric pressure corona discharge ionization (APCDI).[31,32]

Ionization characteristics of DART

The notable reactions observed in DART were oxidations involving oxygen attachment and hydrogen loss. As described above, those oxidation processes in DART are most likely attributable to reactions with HO$^\bullet$. It can be presumed, therefore, that the analyte ionization area between the DART source exit and the mass spectrometer orifice includes a number of active oxygens such as HO$^\bullet$. This hypothesis is supported by the appearance of HCO_2^-, HCO_4^- and $COO^-(COOH)$ as typical negative background ions. It has been found in previous studies of kinetics and atmospheric pressure DC negative corona discharges that the formation of HCO_2^-, HCO_4^- and $COO^-(COOH)$ in the discharge area is attributable to discharge byproducts such as O_3 and HO$^\bullet$ as well as CO originating from electrons having energy between 5 and 10 eV.[31,33] Taking those previous studies into account, Fig. 4 shows the proposed sequential reactions for the formation of O_3, HO$^\bullet$, CO and the resulting negative background ions in DART involved excited He, He(2^3S) having 19.8 eV, as an energy source. The elementary processes shown in Fig. 4 are summarized in Table 2. Collisions of He(2^3S) with O_2 can occur homolytically and heterolytically in terms of bond dissociation to form an O atom in a ground-level triplet state, O(^{3}P), and the O^- ion, respectively (reactions a and e in Fig. 4).[34] The oxygen atom O(^{3}P) can combine rapidly with O_2 to generate ozone O_3 (reaction b in Fig. 4),[34] whereas O^- ion reacts with H_2O resulting in the formation of HO^- ions

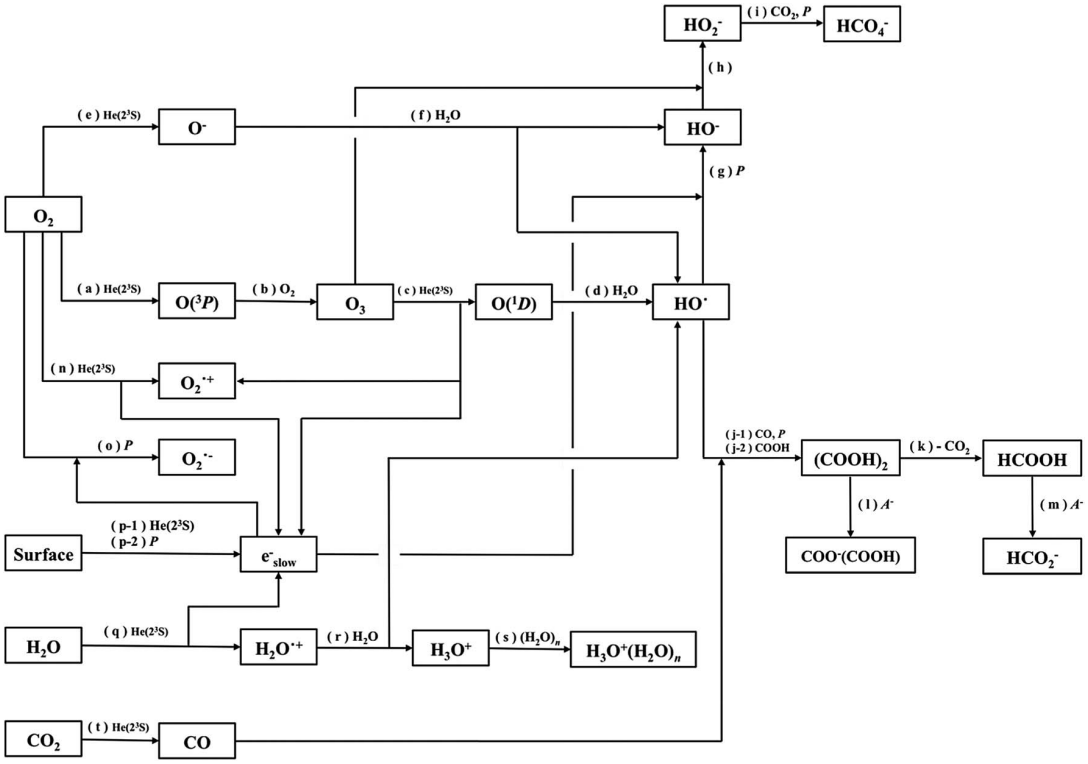

Fig. 4 Proposed sequential reactions for the formation of O_3, HO$^\bullet$, CO and background ions such as $H_3O^+(H_2O)_n$, $O_2^{\bullet-}$, HCO_2^-, HCO_4^- and $COO^-(COOH)$ in DART using He gas.

Table 2 Elementary processes for the formation of O_3, $HO^{\bullet}$, CO and background ions including $H_3O^+(H_2O)_n$, O_2^-, HCO_2^-, HCO_4^- and $COO^-(COOH)$ in DART using He gas[a]

	Reaction	Ref.
a	$O_2 + He(2^3S) \rightarrow O(^3P) + O(^1D) + He(1^1S)$	34
b	$O(^3P) + O_2 + P \rightarrow O_3 + P$	34
c	$O_3 + He(2^3S) \rightarrow O(^1D) + O_2^{\bullet+} + e_{slow}^- + He(1^1S)$	—
d	$O(^1D) + H_2O \rightarrow 2HO^{\bullet}$	34
e	$O_2 + He(2^3S) \rightarrow O^- + O^+ + He(1^1S)$	—
f	$O^- + H_2O \rightarrow HO^- + HO^{\bullet}$	35
g	$HO^{\bullet} + e_{slow}^- + P \rightarrow HO^- + P$	—
h	$HO^- + O_3 \rightarrow HO_2^- + O_2$	26
i	$HO_2^- + CO_2 + P \rightarrow HCO_4^- + P$	36
j-1	$HO^{\bullet} + CO \rightarrow COOH$	37
j-2	$2COOH \rightarrow (COOH)_2$	37
k	$(COOH)_2 \rightarrow HCOOH + CO_2$	37,38
l	$(COOH)_2 + A^- \rightarrow COO^-(COOH) + HA$	—
m	$HCOOH + A^- \rightarrow HCO_2^- + HA$	—
n	$O_2 + He(2^3S) \rightarrow O_2^{\bullet+} + e_{slow}^- + He(1^1S)$	39
o	$O_2 + e_{slow}^- + P \rightarrow O_2^{\bullet-} + P$	40,41
p-1	$Surface + He(2^3S) \rightarrow surface + e_{slow}^- + He(1^1S)$	4
p-2	$e_{fast}^- + P \rightarrow e_{low}^- + P$	—
q	$H_2O + He(2^3S) \rightarrow H_2O^{\bullet+} + e_{slow}^- + He(1^1S)$	4
r	$H_2O^{\bullet+} + H_2O \rightarrow H_3O^+ + HO^{\bullet}$	4
s	$H_3O^+ + (H_2O)_n \rightarrow H_3O^+(H_2O)_n$	4
t	$CO_2 + He(2^3S) \rightarrow CO + O + He(1^1S)$	39

[a] P: third body (N_2 and O_2), A^-: negative ion which has a higher proton affinity than $COO^-(COOH)$ and HCO_2^-.

(reaction f in Fig. 4).[35] The reaction of HO^- with O_3 brings about the formation of HCO_4^- *via* HO_2^- as an intermediate further reacting with CO_2 (reactions h and i in Fig. 4).[26,36] It has been reported that O_3 molecules can dissociate with an energy above 3.87 eV to produce an O atom in an excited singlet state, $O(^1D)$,[34] which is likely achieved involving $He(2^3S)$ (reaction c in Fig. 4). A subsequent reaction of $O(^1D)$ with H_2O leads to the formation of $HO^{\bullet}$ (reaction d in Fig. 4).[34] The radical species $HO^{\bullet}$ can also be formed *via* reactions forming HO^- and H_3O^+ (reactions f and r in Fig. 4).[35,4] The formation of $COO^-(COOH)$ and HCO_2^- most likely originates from an association reaction of $HO^{\bullet}$ with CO (reaction j in Fig. 4).[37] CO can form *via* the dissociation of CO_2 with an energy above 8.3 eV (reaction t in Fig. 4).[41] It is most likely that the sequential reactions shown in Fig. 4 can occur inside a DART source, and the resulting $HO^{\bullet}$ are introduced into the analyte ionization area by the He gas flow, independent of the polarity of the voltage applied to the grid electrode of the DART source exit. Therefore, the oxidation reactions due to $HO^{\bullet}$ can occur easily in both positive- and negative-ion modes.

Based on these results, the ionization characteristics in DART can be summarized as follows. The thermal desorption of condensed-phase analytes, $M_{(solid)}$, results in the formation of gas-phase analytes, $M_{(gas)}$, and fragments $[M - m]_{(gas)}$ due to pyrolysis. The resulting gaseous species $M_{(gas)}$ and $[M - m]_{(gas)}$ are ionized as $[M \pm H]^{\pm}$ and $[M - m \pm H]^{\pm}$ *via* (de)protonation reactions involving the typical background ions $H_3O^+(H_2O)_n$ and $O_2^{\bullet-}$ and slow electrons (1–1.5 eV). Deprotonated analytes $[M \pm H]^{\pm}$ having excess energies can lead to fragmentation with loss of neutral species m to form $[M - m \pm H]^{\pm}$. The species $M_{(gas)}$ can also react with $He(2^3S)$, $O_2^{\bullet+}$ and thermal electrons ($\approx$0 eV) and several negative background ions R^- ($O_2^{\bullet-}$, HCO_2^-, NO_2^- and $COO^-(COOH)$) to produce molecular ions $M^{\bullet\pm}$ and adduct ions $[M + R]^-$, respectively. In contrast, the analytes which tend to be oxidized by $HO^{\bullet}$ can be ionized as (de)protonated analytes with O attachment and/or 2H loss, *i.e.*, $[M + nO \pm H]^{\pm}$ and/or $[M - 2H - H]^-$. The ionization processes occurring in DART and the resulting product ion species are shown in Fig. 5.

Conclusions

The positive and negative ionization characteristics of 20 different α-amino acids were investigated using Direct Analysis in Real Time (DART) mass spectrometry. All of the amino acids

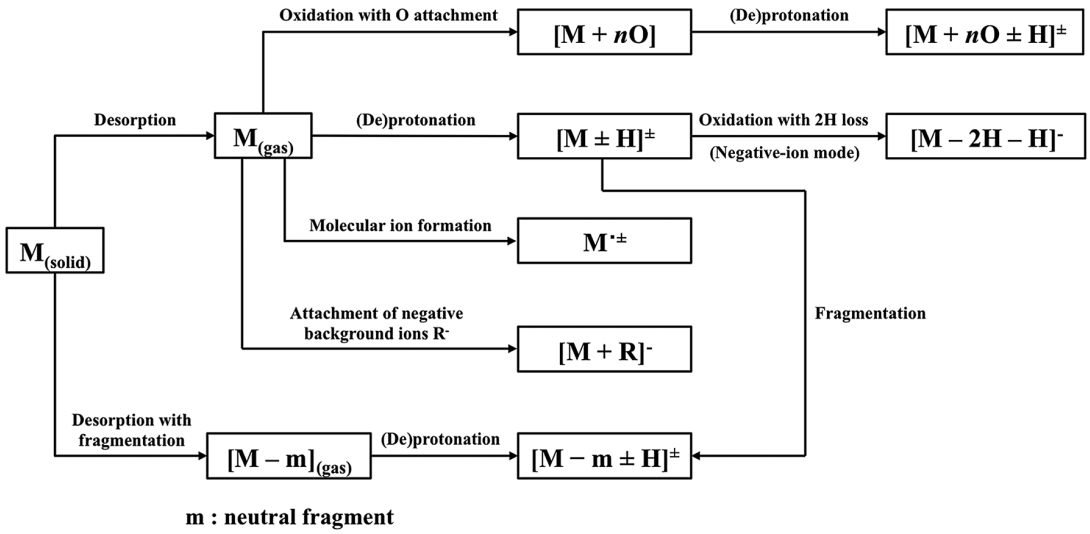

Fig. 5 Summary of the ionization behavior in DART.

except Arg were ionized *via* various reactions depending on the physicochemical and/or structural properties of the individual amino acids, as follows.

(1) (De)protonation of almost all of the amino acids except Arg *via* proton transfer reactions with the typical background ions $H_3O^+(H_2O)_n$ and $O_2^{\bullet -}$ and resonant electron capture by M.

(2) Molecular cation formation of almost all of the amino acids except Arg.

(3) Molecular anion formation of specific amino acids such as Asn and Asp.

(4) Pyrolysis of Glu and Gln.

(5) Fragmentation of Tyr and Asp due to excess energy obtained *via* ionization reactions.

(6) Oxygen attachment of sulfur-containing, aromatic and aromatic heterocyclic amino acids.

(7) Hydrogen loss of aliphatic or non-ionic amino acids.

(8) Attachment of negative background ions R^- ($O_2^{\bullet -}$, HCO_2^-, NO_2^- and $COO^-(COOH)$) for almost all of the amino acids to form $[M + R]^-$.

Oxygen attachment and hydrogen loss can be interpreted as oxidation processes involving active oxygens such as hydroxyl radicals $HO^{\bullet}$. The results suggest, therefore, that analyte ionization in DART can be oxidatively influenced by $HO^{\bullet}$.

Acknowledgements

This work was supported by Grants-in-Aid for Scientific Research (C) (23550101 and 24619005) from the Ministry of Education, Culture, Sports, Science and Technology of Japan.

References

1 S. Soparawalla, G. A. Salazar, R. H. Perry, M. Nicholas and R. G. Cooks, *Rapid Commun. Mass Spectrom.*, 2009, **23**, 131–137.
2 R. R. Steiner and R. L. Larson, *J. Forensic Sci.*, 2009, **54**, 617–622.
3 C. Petucci, J. Diffendal, D. Kaufman, B. Mekonnen, G. Terefenko and B. Mussleman, *Anal. Chem.*, 2007, **79**, 5064–5070.
4 R. B. Cody, J. A. Laramee and H. D. Durst, *Anal. Chem.*, 2005, **77**, 2297–2302.
5 E. S. Chernetsova, G. E. Morlock and I. A. Revelsky, *Russ. Chem. Rev.*, 2011, **80**, 235–255.
6 R. B. Cody, *Anal. Chem.*, 2009, **81**, 1101–1107.
7 R. B. Cody and A. J. Dane, *J. Am. Soc. Mass Spectrom.*, 2013, **24**, 329–334.
8 E. P. Hunter and S. G. Lias, *J. Phys. Chem. Ref. Data*, 1998, **27**, 413–656.
9 C. M. Jones, M. Bernier, E. Carson, K. E. Colyer, R. Metz, A. Pawlow, E. D. Wischow, I. Webb, E. J. Andriole and J. C. Poutma, *Int. J. Mass Spectrom.*, 2007, **267**, 54–62.
10 R. J. O'Hair, J. M. Bowie and S. Gronert, *Int. J. Mass Spectrom. Ion Processes*, 1992, **117**, 23–36.
11 P. H. Cannington and N. S. Ham, *J. Electron Spectros. Relat. Phenom.*, 1983, **32**, 139–151.
12 L. Klasinc, *J. Electron Spectros. Relat. Phenom.*, 1976, **8**, 161–164.
13 M. A. Slifkin and A. C. Allison, *Nature*, 1967, **215**, 949.
14 K. Koyanagi, Y. Kita and M. Tachikawa, *Eur. Phys. J. D*, 2012, **66**, 121.
15 M. J. Travers, D. C. Cowles and G. B. Ellison, *Chem. Phys. Lett.*, 1989, **164**, 449–455.
16 D. Voigt and J. Schmidt, *Biomed. Mass Spectrom.*, 1978, **5**, 44–46.
17 Y. V. Vasil'ev, B. J. Figard, V. G. Voinov, D. F. Barofsky and M. L. Deinzer, *J. Am. Chem. Soc.*, 2006, **128**, 5506–5515.
18 A. M. Scheer, P. Mozejko, G. A. Gallup and P. D. Burrow, *J. Chem. Phys.*, 2007, **126**, 174301.
19 Y. V. Vasil'ev, B. J. Figard, D. F. Barofsky and M. L. Deinzer, *Int. J. Mass Spectrom.*, 2007, **268**, 106–121.
20 S. Denifl, H. D. Flosadóttir, A. Edtbauer, O. Ingólfsson, T. D. Märk and P. Scheier, *Eur. Phys. J. D*, 2010, **60**, 37–44.
21 R. B. Cody, *Anal. Chem.*, 2009, **81**, 1101–1107.
22 J. Douda and V. A. Basiuk, *J. Anal. Appl. Pyrolysis*, 2000, **56**, 113–121.
23 W. M. Lagna and P. S. Callery, *Biomed. Mass Spectrom.*, 1985, **12**, 699–703.
24 J. B. Mudd, R. Leavitt, A. Ongun and T. T. McManus, *Atmos. Environ.*, 1969, **3**, 669–682.
25 T. Kotiaho, M. N. Eberlin, P. Vainiotalo and R. Kostiainen, *J. Am. Soc. Mass Spectrom.*, 2000, **11**, 526–535.
26 V. K. Sharma and N. J. D. Graham, *Ozone: Sci. Eng.*, 2010, **32**, 81–90.
27 K. Takamoto and M. R. Chance, *Annu. Rev. Biophys. Biomol. Struct.*, 2006, **35**, 251–276.
28 W. A. Pryor, D. H. Giamalva and D. F. Church, *J. Am. Chem. Soc.*, 1984, **106**, 7094–7100.
29 L. Song, A. B. Dykstra, H. Yao and J. E. Bartmess, *J. Am. Soc. Mass Spectrom.*, 2009, **20**, 42–50.
30 R. M. Le Lacheur and W. H. Graze, *Environ. Sci. Technol.*, 1996, **30**, 1072–1080.
31 K. Sekimoto, M. Sakai and M. Takayama, *J. Am. Soc. Mass Spectrom.*, 2012, **23**, 1109–1119.
32 K. Sekimoto, N. Matsuda and M. Takayama, *Mass Spectrometry*, 2013, **2**, A0020.
33 K. Sekimoto and M. Takayama, *Eur. Phys. J. D*, 2010, **60**, 589–599.
34 D. J. Jacob, *Introduction to Atmospheric Chemistry*, Princeton University Press, Princeton, New Jersey, 1st edn, 1999, pp. 163–171.
35 F. C. Fehsenfeld and E. E. Ferguson, *J. Chem. Phys.*, 1974, **61**, 3181–3193.
36 T. McAllister, A. J. C. Nicholson and D. L. Swingler, *Int. J. Mass Spectrom. Ion Phys.*, 1978, **27**, 43–48.
37 B. J. Finlayson-Pitts and J. N. Pitts, Jr, *Chemistry of the Upper and Lower Atmosphere*, Academic Press, San Diego, 1st edn, 2000, pp. 137–138.
38 N. Getoff, *Int. J. Hydrogen Energy*, 1994, **19**, 667–672.
39 D. R. Lide, *Handbook of Chemistry and Physics*, CRC Press, Boca Raton, 88th edn, 2007, pp. 9–56.
40 J. L. Pack and A. V. Phelps, *J. Chem. Phys.*, 1966, **44**, 1870–1883.
41 L. M. Chanin, A. V. Phelps and M. A. Bionidi, *Phys. Rev.*, 1962, **128**, 219–230.